



# Green biochar-based adsorbent for radiocesium and Cu, Ni, and Pb removal

Lukáš Mészáros<sup>1</sup> · Matej Šuránek<sup>1</sup> · Zuzana Melichová<sup>1</sup> · Vladimír Frišták<sup>2</sup> · Libor Ďuriška<sup>3</sup> · Mária Kaňuchová<sup>4</sup> · Gerhard Soja<sup>5,6</sup> · Martin Pipíška<sup>2</sup>

Received: 18 May 2023 / Accepted: 6 August 2023 / Published online: 23 August 2023  
© The Author(s) 2023

## Abstract

Thermochemical conversion of garden waste to biochar was carried out to prepare a green adsorbent for the removal of Cs, Cu, Ni, and Pb, which was characterized by XPS, SEM–EDX, and FT-IR analyses. The biochar's adsorption capacity was 20.5(Cs), 25.2(Cu), 12.4(Ni), and 45.9(Pb) mg g<sup>-1</sup> and demonstrated satisfactory performance for different pH values. The kinetics data evaluation revealed that besides chemisorption, intraparticle diffusion contributes to metal removal. Moreover, the physical and structural properties of biochar play an important role in adsorption. Results indicate the suitability of using GW biochar as an alternative sorbent for both radionuclides and metal extraction.

**Keywords** Biochar · Garden waste · Radiocesium · Heavy metals · Adsorption

## Introduction

In the last years, increasing pressure has been raised for sustainable solutions to environmental problems. Biochar has gained considerable attraction as an inexpensive material that complements the green paradigm for a number of

possible applications, including soil improvement [1, 2], sequestration of carbon [3], and wastewater treatment [4, 5].

Among the various specific processes for the treatment of metal and radionuclide-polluted effluents, adsorption using activated carbon is the most commonly applied for water treatment in chemical engineering [6, 7]. As a wastewater adsorbent, biochar from lignocellulose waste biomass is considered an option for activated carbon for the elimination of a variety of pollutants involving radionuclides (<sup>137</sup>Cs, Sr, U) [8–10], and metal cations such as Cd<sup>2+</sup>, Cu<sup>2+</sup>, Mn<sup>2+</sup>, Ni<sup>2+</sup>, Pb<sup>2+</sup>, and Zn<sup>2+</sup> [11–14]. A meta-analysis reported by Alhashimi and Aktas [15] found that biochar as a sorbent has a lower global warming potential impact (–0.9 kg CO<sub>2</sub>eq kg<sup>-1</sup> vs. 6.6 kg CO<sub>2</sub>eq kg<sup>-1</sup>), a lower energy requirement (6.1 MJ kg<sup>-1</sup> vs. 97 MJ kg<sup>-1</sup>), and a lower environmental impact in comparison to activated carbons. Authors also found that the biochar adsorptive capacities for toxic metals can be comparable to or higher than the adsorption capacity of activated carbon. As was pointed out by several authors [16, 17], the biochar adsorptive capacities and the adsorption mechanism of toxic metals and radionuclides are predominantly affected by the raw material employed for biochar preparation and production conditions. Therefore, one way to achieve acceptable adsorption performance without the need for biochar post-production modification (which compromises sustainability) is to search for a suitable and widely

✉ Martin Pipíška  
martin.pipiska@truni.sk

- <sup>1</sup> Department of Chemistry, Faculty of Natural Sciences, Matej Bel University, Tajovskeho 40, Banská Bystrica 97401, Slovak Republic
- <sup>2</sup> Department of Chemistry, Faculty of Education, Trnava University in Trnava, Priemyselná 4, P.O. Box 9, Trnava 918 43, Slovak Republic
- <sup>3</sup> Institute of Materials Science, Faculty of Materials Science and Technology in Trnava, Slovak University of Technology in Bratislava, J. Bottu 25, Trnava 917 24, Slovak Republic
- <sup>4</sup> Institute of Earth Resources, Faculty of Mining, Ecology, Process Control and Geotechnologies, Technical University of Košice, Park Komenského 19, Košice 042 00, Slovak Republic
- <sup>5</sup> Energy Department, AIT Austrian Institute of Technology GmbH, Konrad-Lorenz- Straße 24, 3430 Tulln an Der Donau, Austria
- <sup>6</sup> Institute for Chemical and Energy Engineering, University of Natural Resources and Life Sciences, Muthgasse 107, 1190 Vienna, Austria

available feedstock that can maximize metal and radionuclide adsorption efficiency by biochar.

Garden waste is a less exploited resource from green areas and is steadily increasing as a result of the extension of urban and green areas [18]. Thermochemical conversion of garden waste consisting of a variety of plant residues (e.g. leaves, branches, cuttings, and grass clippings) into biochar overcomes the problems caused by their composting, land-filling, and incineration [16]. The use of green waste biochar as a high-value-added product for water purification has not been intensively investigated so far [4, 19], whereas a few studies were focused on its use as soil amendment [18, 20].

Therefore, in the present research, thermochemical conversion of garden waste (GW) biomass to biochar was carried out to prepare green adsorption material for both heavy metals (Cu, Ni, Pb) and radionuclides ( $^{137}\text{Cs}$ ). The biochar-based adsorbent was precisely characterized (SEM, EDX elemental mapping, XPS, FT-IR), used to adsorb Cs, Cu, Ni, and Pb cations from aqueous solutions, and the equilibrium and kinetic behavior were systemically evaluated using batch adsorption experiments. Moreover, the impact of biochar characteristics on Cs, Cu, Ni, and Pb removal was discussed.

## Experimental

### Biochar production and characterization

Garden waste (mainly woody and leaf biomass) was obtained from the Austrian Institute of Technology (Tulln, Austria), shredded into small pieces (<2 cm), and pyrolyzed in a modified laboratory reactor applying a slow pyrolysis process in a batch mode at a maximal working temperature of 500 °C. The required temperature was maintained for 2 h and inert conditions were provided by  $\text{N}_2$  as a purge gas. After pyrolysis, GW biochar was rinsed in Milli-Q-grade water (<0.4  $\mu\text{S cm}^{-1}$ , Millipore, USA), dried (90 °C) to a constant weight, and ground. After sieve analysis fraction 0.5–1 mm was selected for adsorption tests.

A combustion-type elemental analyzer (Carlo Erba Instruments) was applied to determine the total C, H, N, and S contents of GW. The chemical properties of biochar (cation exchange capacity CEC, electrical conductivity EC, and pH) were determined by standard approaches. Before measuring pH, biochar and deionized water were mixed (ratio 1:2.5) for 60 min and then stabilized for 60 min. The  $\text{BaCl}_2$  method was applied to measure the CEC value of GW biochar. The biochar point of zero charge ( $\text{pH}_{\text{pzc}}$ ) was measured employing the drift method [21]. The BET surface area of GW biochar and pore properties were analyzed by  $\text{N}_2$  gas sorption using a Quantachrome Nova analyzer.

EDX microanalysis and inspection of the microstructure and morphology of the biochar sample were performed using

a JEOL JSM7600F scanning electron microscope (Japan) at 20 kV in secondary electron mode. Infrared absorption spectra (within the range of 4000–400  $\text{cm}^{-1}$ ) of biochar samples before and after Cs, Cu, Ni, and Pb adsorption were measured using the Nicolet iS50 FTIR spectrometer with ATR module. The biochar surface chemical analysis was realized using an XPS analyzer (SPECS GmbH, Germany) with PHOIBOS 100 SCD and a non-monochromatic X-ray source according to the procedure described in detail in our previous work [4].

### Metal adsorption experiments

The working solutions of Cu, Ni and Pb (300  $\text{mg L}^{-1}$ ) used in all adsorption tests were prepared from  $\text{CuSO}_4 \cdot 5\text{H}_2\text{O}$  (Mikrochem, Slovakia),  $\text{Pb}(\text{NO}_3)_2$  (Mikrochem, Slovakia), and  $\text{NiSO}_4 \cdot 7\text{H}_2\text{O}$  (Acros Organics). The batch adsorption trials were realized in Erlenmeyer flasks (0.25 L), by adding GW biochar (0.1 g) to 50 mL of a corresponding metal solution with an initial concentration ranging from 10 to 300  $\text{mg g}^{-1}$  and pH from 2.0 to 8.0. Erlenmeyer banks were agitated in an orbital shaker ES–20/60 (Biosan, Latvia) at 25 °C and 200 rpm. At the end of the experiments, the suspensions were filtered and the metal contents remained in the solution were measured using an atomic absorption spectrometer with acetylene–air flame atomization (AVANTA  $\Sigma$ , GBC Scientific, Melbourne, Australia). The GBC Avanta v.2.0 software was applied for data processing. Standard Cu, Ni, and Pb solutions (Specpure) were applied to regularly monitor the response of the instrument. The adsorption capacity  $Q$  ( $\text{mg g}^{-1}$ ) was calculated according to Eq. (1):

$$Q = \frac{(c_0 - c_t)V}{m} \quad (1)$$

where  $c_t$  is the concentration of metal in the time  $t$  ( $\text{mg L}^{-1}$ ),  $c_0$  is the initial metal concentration ( $\text{mg L}^{-1}$ ),  $V$  is the volume of solution (L), and  $m$  weight of biochar in solution (g).

### Radiocesium adsorption experiments

The working Cs solution was prepared in deionized water from CsCl (analytical grade; Sigma- Aldrich, USA). The batch adsorption trials were realized by suspending 0.1 g of GW biochar in cesium solution labeled with  $^{137}\text{CsCl}$  ( $\text{CsCl}$  20  $\text{mg L}^{-1}$  in 3  $\text{g L}^{-1}$  HCl, 5.406 MBq  $\text{mL}^{-1}$ ; Czech Metrological Institute, Czech Republic) at the starting concentration from 13 to 400  $\text{mg L}^{-1}$  and pH from 2.0 to 8.0. The contents of the flasks were stirred on a reciprocal shaker (200 rpm, 25 °C). After 24 h or after the necessary exposure

time in the case of kinetics assays, the suspensions were filtered with a 0.45  $\mu\text{m}$  filter and  $^{137}\text{Cs}$  radioactivity in both biochar and filtrates was quantified. The radiometric analysis was conducted using 54BP54/2-X scintillation gamma-spectrometer with a well-type NaI(Tl) detector (Scionix, The Netherlands) and ScintiVision-32 software (Ortec, USA) was applied for data processing. Characteristic  $\gamma$ -ray peak for  $^{137}\text{Cs}$  ( $E_\gamma = 661.64$  keV) was chosen for energy and efficiency calibration. A standard  $^{137}\text{CsCl}$  solution with known radioactivity was used for calibration along with the radionuclide half-life ( $^{137}\text{Cs}$   $T_{1/2} = 30.17$  y). The amount of  $\text{Cs}^+$  adsorbed  $Q$  ( $\text{mg g}^{-1}$ ) was calculated by Eq. 1.

## Data modeling

The isotherm and kinetic tests were realized to understand the thermodynamic adsorption behavior of biochar. Obtained dynamics data were evaluated by both reaction-controlled kinetics and diffusion-controlled kinetics models, namely the pseudo-second-order model (PSO) [22] given by non-linear Eq. (2):

$$Q_t = (Q_e^2 k_2 t) / (1 + k_2 Q_e t) \quad (2)$$

where  $k_2$  is the pseudo-second-order rate constant ( $\text{g mg}^{-1} \text{min}^{-1}$ ),  $Q_t$  and  $Q_e$  are the amount of Cs, Cu, Ni, and Pb ( $\text{mg g}^{-1}$ ) adsorbed at any time  $t$  (min) and equilibrium, respectively, and intraparticle diffusion model (IDM) [23] given by Eq. (3):

$$Q_t = k_i t^{0.5} + I \quad (3)$$

where  $k_i$  is the intraparticle diffusion rate constant ( $\text{mg g}^{-1} \text{min}^{-0.5}$ ),  $Q_t$  is the amount of Cs, Cu, Ni, and Pb ( $\text{mg g}^{-1}$ ) adsorbed at time  $t$  (min), and  $I$  represent a constant that reflects the thickness of the boundary layer ( $\text{mg g}^{-1}$ ).

Equilibrium data were fitted with Langmuir monolayer adsorption isotherm (4) [24], and experimental Freundlich (5) isotherm [25]. The non-linear equations are given as follows:

$$Q_e = \frac{b Q_{max} C_e}{1 + b C_e} \quad (4)$$

$$Q_e = K C_e^{(1/n)} \quad (5)$$

where  $b$  is constant referring to the affinity of binding sites ( $\text{L mg}^{-1}$ ),  $Q_{max}$  indicates the maximum adsorption capacity of GW biochar ( $\text{mg g}^{-1}$ ), Freundlich constant  $K$  [ $(\text{mg g}^{-1}) (\text{L mg}^{-1})^{1/n}$ ] referring adsorption capacity and  $1/n$  is non-dimensional constant referring to the adsorption intensity.

The parameters of PSO and isotherm models were calculated using the non-linear regression analysis (OriginPro

2016, OriginLab Corporation, USA). The chemical equilibrium software Visual MINTEQ (version 3.1) was used for the calculation of Cs, Cu, Ni, and Pb speciation in solution [26].

## Results and discussion

### General properties of biochar

The basic physicochemical characteristics of biochar produced by the slow pyrolysis of garden waste (woody and foliar biomass) are given in Table 1. GW biochar was characterized by the high C content (80.5%), whereas the level of H, N, and S was as expected low (1.64, 0.65, and 0.13%). The biochar chemical composition is highly depended on the pyrolysis conditions, and the low H/C atomic ratio (0.245) is due to structural transformations of cellulose, hemicelluloses, and lignin and the loss of hydrophilic surface functional moieties [27] which occurs at 500 °C in association with an increased aromaticity and condensation degree. Produced biochar had slightly higher electrical conductivity and was alkaline in nature ( $\text{pH} = 9.10$ ). The considerable alkalinity is explained by the presence of inorganic constituents in the biochar (see results below), especially salts of alkali (K) and alkaline earth elements (Ca and Mg). The cation exchange capacity (CEC) was 125  $\text{mmol kg}^{-1}$  indicating the good ability of GW biochar to hold metal cations. The BET surface area was 6.69  $\text{m}^2 \text{g}^{-1}$ . As shown by several authors, BET area increases with elevating the temperature of pyrolysis, and in general biochar prepared at temperatures below 500 °C has a specific surface area of less than 10  $\text{m}^2 \text{g}^{-1}$  [27, 28]. The total pore volume was 0.010  $\text{cm}^3 \text{g}^{-1}$  and as can be seen from Table 1, a significant part was represented by mesopores (0.007  $\text{cm}^3 \text{g}^{-1}$ ).

The example SEM image in Fig. 1a highlights the structure and morphology of biochar produced from garden waste namely leaf and wood biomass. It is obvious that biochar exhibits an uneven surface with a pore structure that displays residual anatomical characteristics and morphology

**Table 1** Basic physicochemical and pore characteristics of GW biochar

Parameter		Parameter	
pH ( $\text{H}_2\text{O}$ )	9.10 ± 0.11	H/C ratio	0.245
CEC ( $\text{mmol kg}^{-1}$ )	125	$\text{CaCO}_3$ (%)	6.60 ± 0.25
EC ( $\text{dS m}^{-1}$ )	1.15 ± 0.02	Density ( $\text{kg L}^{-1}$ )	0.34
C %	80.5	$V_{\text{meso}}$ ( $\text{cm}^3 \text{g}^{-1}$ )	0.007
H %	1.64	$V_{\text{micro}}$ ( $\text{cm}^3 \text{g}^{-1}$ )	0.003
N %	0.65	$V_{\text{pore}}$ ( $\text{cm}^3 \text{g}^{-1}$ )	0.010
S %	0.13	$\text{SSA}_{\text{BET}}$ ( $\text{m}^2 \text{g}^{-1}$ )	6.69

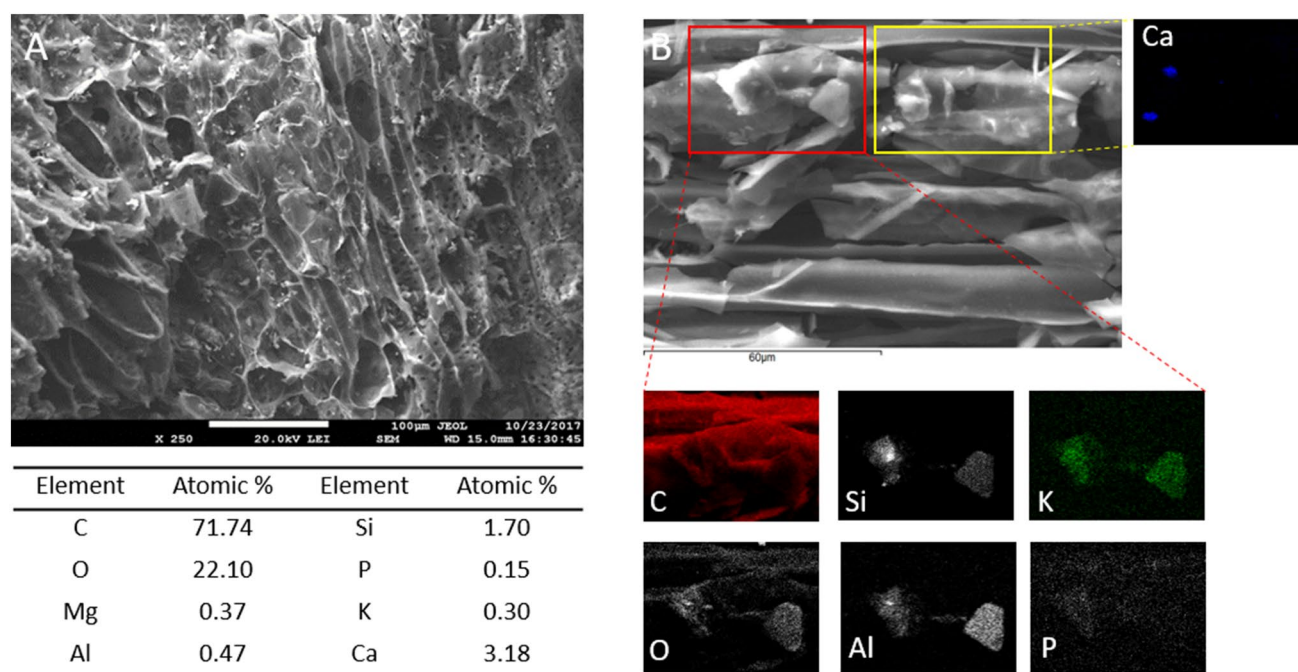


**Fig. 1** Scanning electron microscopy micrographs **a**, EDX **b** images, and elemental composition of GW biochar. The EDX maps of elemental distribution depict the elemental composition (C, O, Si, Al, K, P, and Ca) of the regions enclosed by the yellow and red lines in panel B

of feedstock biomass. Among others, tracheids and lateral communication between tracheids are widely observed. The slit-shaped pores from vesicles formed during pyrolysis at 500 °C are also well visible (Fig. 1a). EDX elemental mapping also showed the occurrence of K, Ca, Mg, P, Si, and Al (Fig. 1b), besides the major bulk biochar elements (C, H, O). Inorganic particles measuring 10–15 μm are present on the surface (Fig. 1b) or can be trapped in the pores. In biochar, these mineral constituents are often present as oxides (e.g. quartz SiO<sub>2</sub>), phosphates (hydroxyapatite (Ca<sub>10</sub>PO<sub>4</sub>)<sub>6</sub>(OH)<sub>2</sub>), carbonates (calcite CaCO<sub>3</sub>) [29] or aluminosilicates (e.g. feldspar) [30] and, as discussed in our previous work [4, 31] can significantly affect the biochar adsorption properties.

XPS analysis gives information on the composition and chemistry of biochar surfaces. The XPS survey spectrum of GW biochar is shown in Fig. 2a. A characteristically robust carbon signal at 284.0 eV (C 1 s) was noticed for GW biochar, as expected, together with a significant amount of oxygen identified at a binding energy of 532.5 eV (O 1 s). In addition, the investigated biochar showed a relatively high abundance of Si (2.24%) and the presence of other elements (Ca, Mg, and N) in amounts below 1% was also confirmed. To investigate the nature of oxygen species on biochar surfaces, high-resolution O 1 s and C 1 s XPS spectra were characterized. The O 1 s band of GW biochar was deconvoluted to these peaks: (i) peak at 529.4 eV representing O atoms in carboxyl groups; (ii) peak at 530.9 eV representing O in anhydrides and esters, and (iii) peak at 532.9 eV

presenting oxygen atoms in carbonyl oxygen in anhydrides and esters and in hydroxyl groups [32–34] (Fig. 2b). The deconvolution of the C 1 s spectra yielded three peaks: (i) peak at 284.36 eV corresponds to graphitized carbon; (ii) peak at 285.54 eV represents carbon in alcohol, phenolic, and ether groups and (iii) peak at 287.72 eV presents carbon in quinone or carbonyl groups (Fig. 2c). The content and types of oxygen functional moieties indicate that biochar produced from garden waste will be a promising adsorbent for both radionuclides and heavy metal ions.

Mid-infrared region (4000–400 cm<sup>-1</sup>) spectral analysis of the garden waste-derived biochar was conducted to determine the main surface functional moieties. Figure 3 shows typical ATR-FTIR spectra of raw and metal-loaded biochar. It is apparent that O–H groups vibrations (3600–3200 cm<sup>-1</sup>) and aliphatic C–H stretch vibrations (2925 cm<sup>-1</sup>) are absent as a consequence of the slow pyrolysis of the feedstock at 500 °C during which dehydration and lignin demethylation and demethoxylation occurred [35]. Nevertheless, the aromatic ν(C=C) band at 1573 cm<sup>-1</sup> and the out-of-plane bending vibrations of the aromatic C–H bond at 875, 809, and 750 cm<sup>-1</sup> have considerable intensity in the GW biochar (Fig. 3). The peaks at 1027 and 1693 cm<sup>-1</sup> correspond to stretching vibrations of C–O and ν(C=O) from carboxylic acids of undecomposed cellulosic and ligneous carbon [36], suggesting the existence of O-containing moieties on the surfaces of GW biochar. The low intensity of these peaks is in agreement with the observations of other authors, who

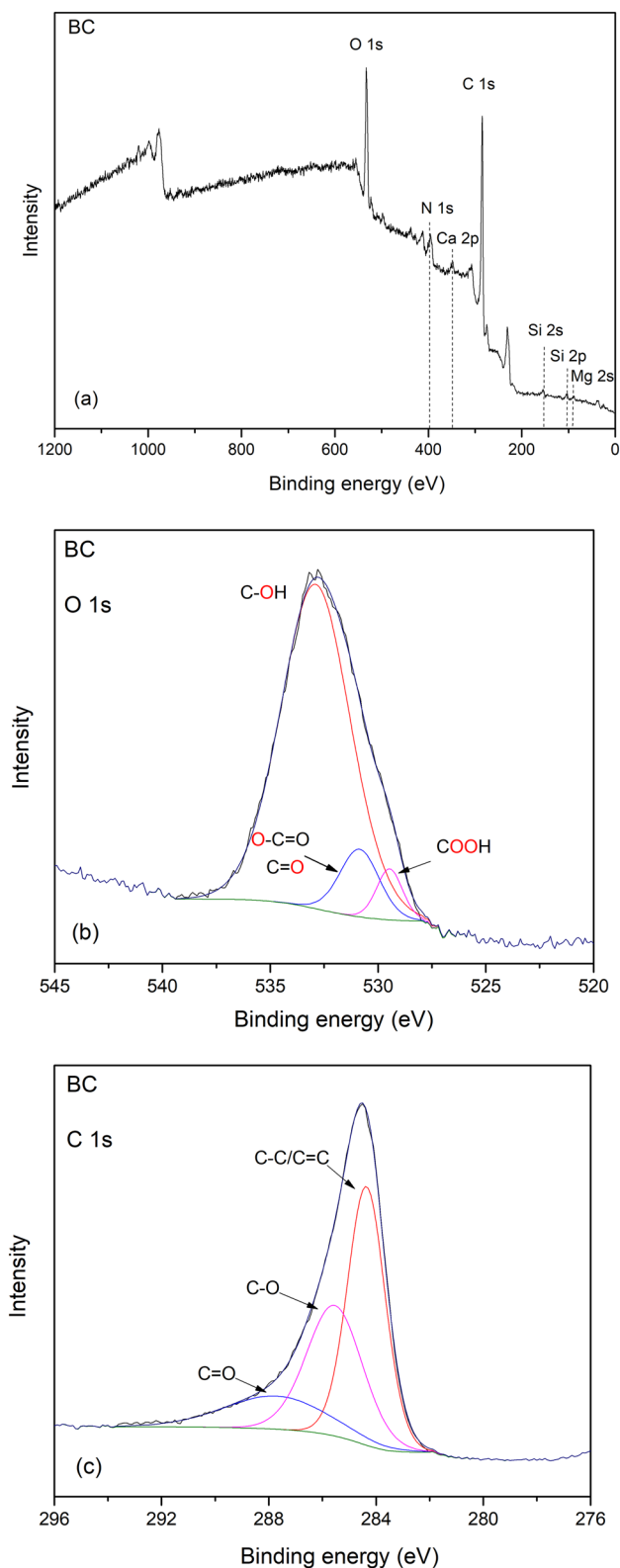


**Fig. 2** Survey XPS spectra **a** and high-resolution O 1s **b** and C 1s **c** spectra of GW biochar

describe that in the case of biochar prepared at temperatures above 500 °C there is a significant reduction of O-containing functional moieties [37]. The contributions of biochar mineral fractions to the spectra are also present in the bands between 1500 and 750  $\text{cm}^{-1}$ . The band at 1401  $\text{cm}^{-1}$  could be attributed to carbonates ( $\text{CO}_3^{2-}$ ), and the band at 1027  $\text{cm}^{-1}$  to the P-O bond of phosphates. The bandwidth of 1200 to 1100  $\text{cm}^{-1}$  could be attributed to  $\nu(\text{Si-O})$  of associated clay minerals.

Determination of garden waste-derived biochar point of zero charge ( $\text{pH}_{\text{pzc}}$ ) was carried out using the pH drift procedure. From plotted graph (Fig. 4), the  $\text{pH}_{\text{pzc}}$  value of 7.2 is clearly identified by crossing the final vs. the initial pH. At solution pHs  $> \text{pH}_{\text{pzc}}$  biochar outer and inner surfaces are negatively charged as a consequence of deprotonating reactions and the attraction of positively charged metal species can take place and contribute to Cs, Cu, Ni, and Pb removal (see discussion below).

The above physicochemical and surface properties indicate an excellent possibility for the separation of radiocesium and Cu, Ni, and Pb ions from contaminated water streams using biochar produced from garden waste.

### Adsorption kinetics of Cs, Cu, Ni, and Pb

The Cu, Ni, and Pb adsorption capacities at different times were investigated. The time progression of adsorption is plotted in Fig. 5, and in all cases, a similar trend of a rapid enhancement in adsorption capacities within the first minutes of the experiment is observed, with a subsequent slow-down in growth and finally a stabilization of the adsorption equilibrium after 24 h. In the case of  $\text{Cs}^+$  ions, the driving force is also higher in the initial phase (0.5–3 h) and  $\text{Cs}^+$  ions bind to the external surfaces with subsequent diffusion of  $\text{Cs}^+$  through the pore texture and subsequent physical and chemical adsorption into the networks of biochar fissures and pores. Palansooriya et al. [9] using the same initial Cs concentration (100  $\text{mg L}^{-1}$ ) obtained identical kinetics progression of Cs adsorption by biochar from wood and biochar from a mixture of wood (40%) and food waste (60%). It is evident that the adsorbed amounts for individual ions decrease in the order  $\text{Pb} > \text{Cu} > \text{Ni} > \text{Cs}$ , indicating a much stronger adsorption capacity for lead (Table 2). A similar kinetic profile for Pb adsorption by the banana stem and leaf biochar was described by Liu et al. [38] with equilibrium attained after 16 h. Mahdi et al. [39] observed that the removal kinetics of Cu by date seed biochar is much faster than Ni, which confirms our data.

To quantitate the initial fast and slow adsorption of Cs, Ni, Cu, and Pb and to identify the adsorption performance, the dynamic data were evaluated by reaction-driven kinetics (PSO, Eq. 2) and diffusion-driven kinetics (IDM, Eq. 3) models. The fitting outputs given in Table 2 and Fig. 5

**Fig. 3** ATR-FTIR spectra of GW biochar before and after Cu, Ni, and Pb (initial concentration:  $300 \text{ mg L}^{-1}$ ) and Cs (initial concentration:  $400 \text{ mg L}^{-1}$ ) adsorption

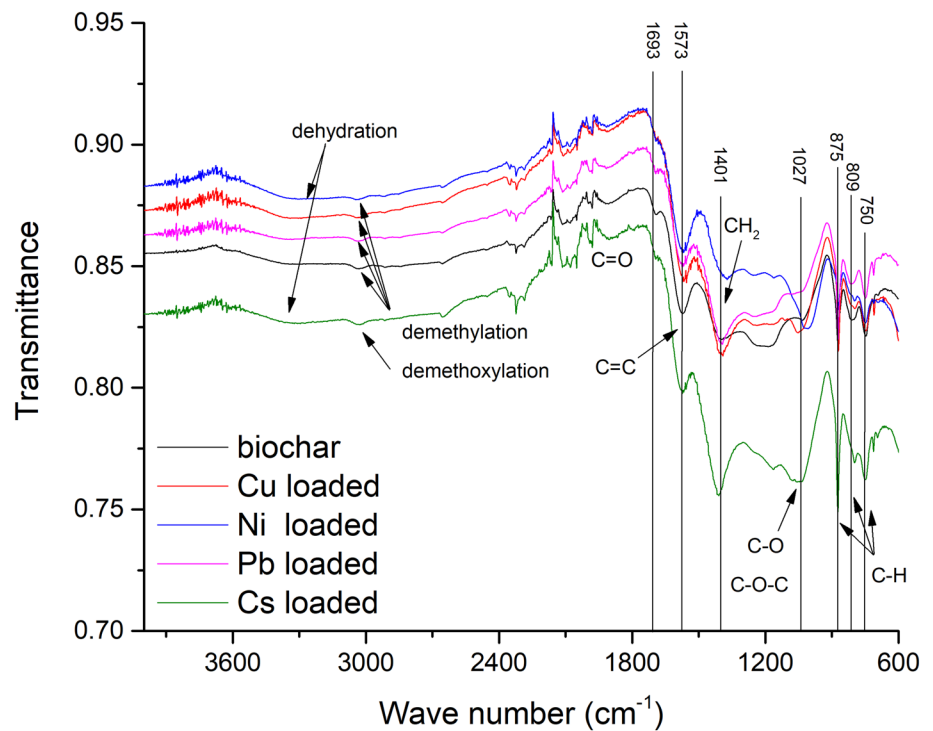
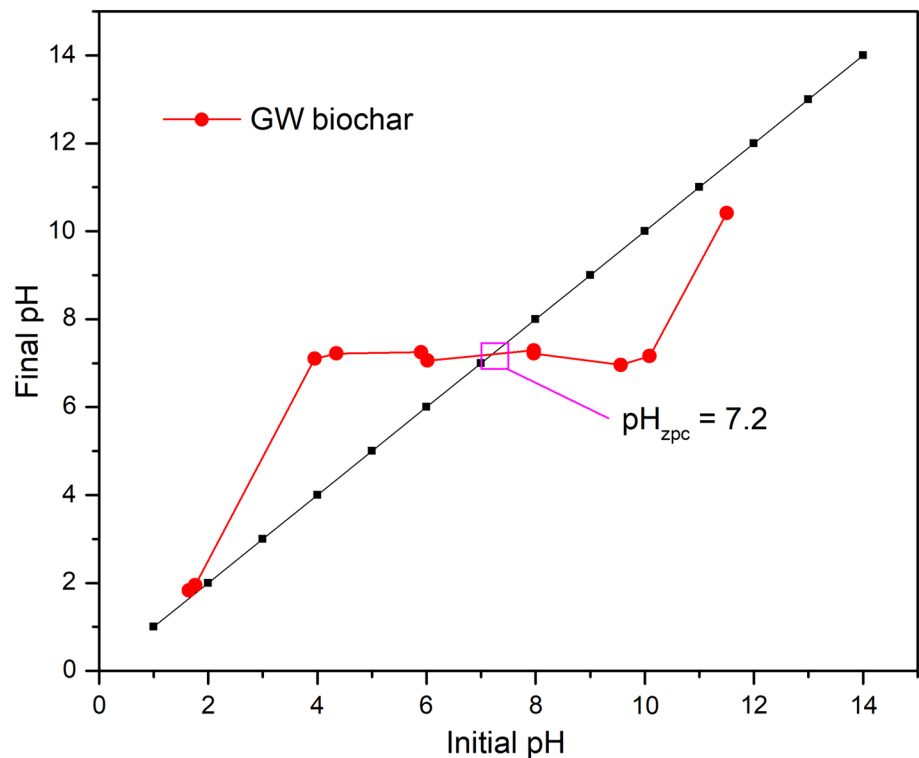


**Fig. 4** Point of zero charge ( $\text{pH}_{\text{zpc}}$ ) of GW biochar



confirm that the PSO model can be considered as the appropriate model describing kinetics adsorption process of Cu, Ni, and Pb onto GW biochar with theoretical  $Q_e$  values of 9.43, 8.38, and  $34.6 \text{ mg g}^{-1}$  and indicate that chemical

reaction (adsorption) participate on metal removal. Based on the recent literature review, the PSO model appeared to best describe the adsorption uptake rate of  $\text{Pb}^{2+}$  and  $\text{Cd}^{2+}$  on biochar surface from banana leaf and stem [38],  $\text{Zn}^{2+}$  on

**Fig. 5** Application of PSO kinetic model for the adsorption of Cs, Cu, Ni, and Pb on GW biochar. (Initial Me concentration: 100 mg L<sup>-1</sup>; pH 6.0 (Cs<sup>+</sup>), 5.2 (Cu<sup>2+</sup>), 5.6 (Ni<sup>2+</sup>), 5.0 (Pb<sup>2+</sup>); biochar dosage 2 g L<sup>-1</sup>; particle size: 0.5–1.0 mm; 25 °C)

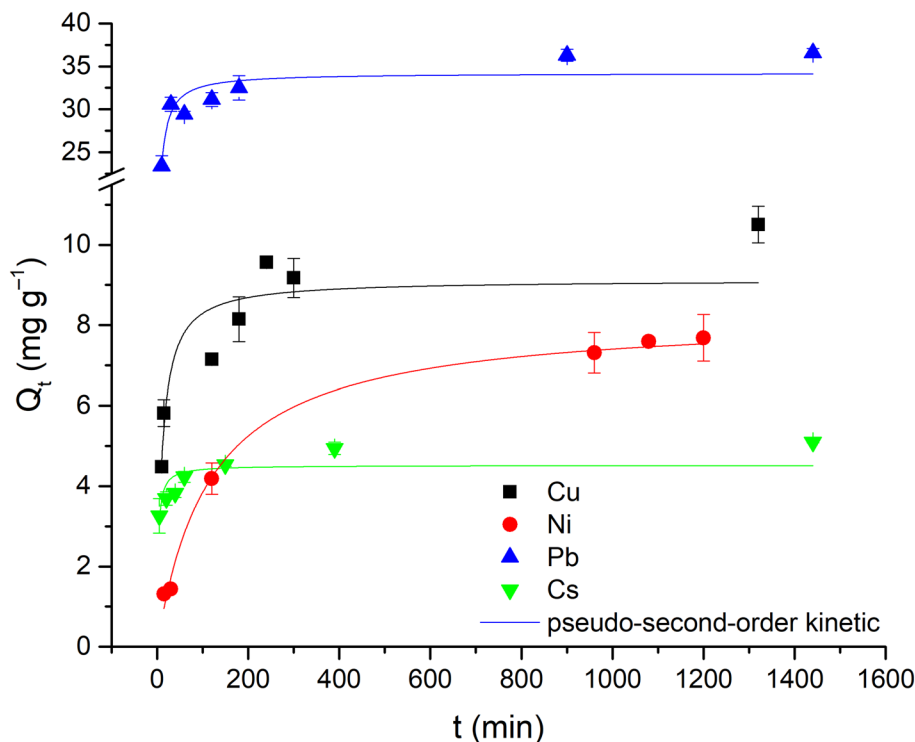


**Table 2** Kinetic parameters of cesium, copper, nickel, and lead adsorption ( $C_0 = 100 \text{ mg L}^{-1}$ ) for garden green waste biochar computed from PSO and IDM models

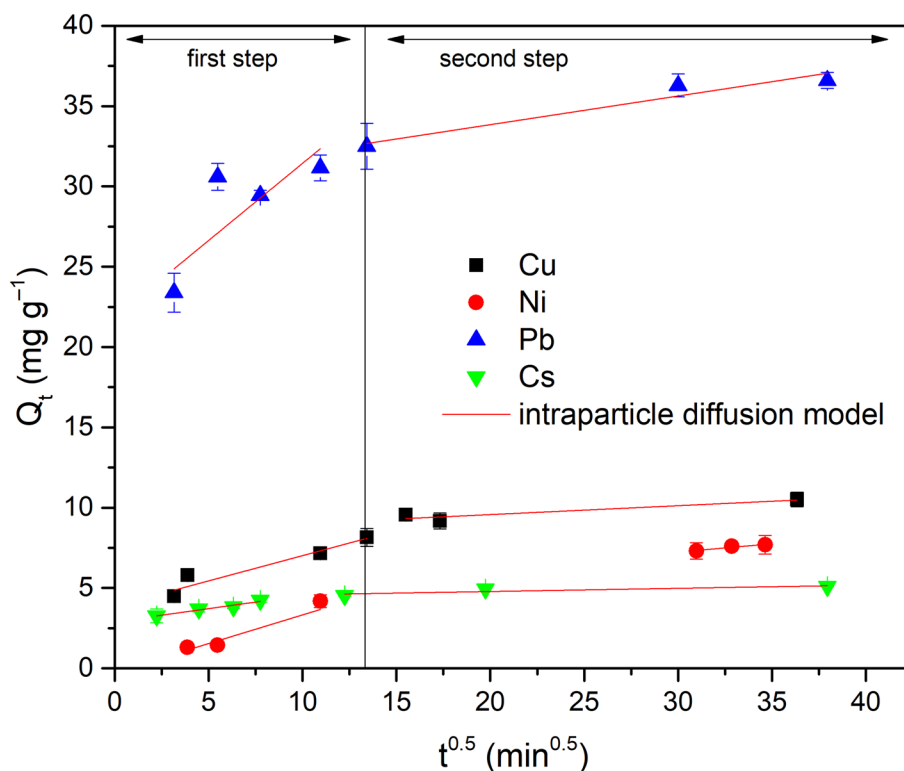
Metal	$Q_{exp}$	Model	Parameter 1	Parameter 2	$R^2$
Cu	10.5	PSO	$Q_e = 9.43 \pm 0.51$	$k_2 = 0.0094 \pm 0.0034$	0.838
		IDM	$k_{i1} = 0.30 \pm 0.07$	$I_1 = 4.05 \pm 0.59$	0.913
			$k_{i2} = 0.06 \pm 0.02$	$I_2 = 8.47 \pm 0.53$	0.869
Pb	36.6	PSO	$Q_e = 34.6 \pm 1.05$	$k_2 = 0.00557 \pm 0.00162$	0.829
		IDM	$k_{i1} = 0.84 \pm 0.48$	$I_1 = 22.9 \pm 3.54$	0.756
			$k_{i2} = 0.18 \pm 0.05$	$I_2 = 30.3 \pm 1.34$	0.935
Ni	7.67	PSO	$Q_e = 8.38 \pm 0.21$	$k_2 = 0.00099 \pm 0.00034$	0.995
		IDM	$k_{i1} = 0.43 \pm 0.08$	$I_1 = -0.59 \pm 0.20$	0.968
			$k_{i2} = 0.90 \pm 0.03$	$I_2 = 4.18 \pm 0.94$	0.927
Cs	5.09	PSO	$Q_e = 4.65 \pm 0.20$	$k_2 = 0.073 \pm 0.031$	0.690
		IDM	$k_{i1} = 0.16 \pm 0.02$	$I_1 = 2.90 \pm 0.13$	0.961
			$k_{i2} = 0.02 \pm 0.01$	$I_2 = 4.41 \pm 0.26$	0.881

$Q_{exp}$  (mg g<sup>-1</sup>);  $k_2$  (g mg<sup>-1</sup> min<sup>-1</sup>);  $Q_e$  (mg g<sup>-1</sup>);  $I$  (mg g<sup>-1</sup>);  $k_i$  (mg g<sup>-1</sup> min<sup>-0.5</sup>)

rice straw biochar [40], Cd<sup>2+</sup> ions on biochar based carbon fertilizer [41] which also confirms that chemical reactions primarily controlled the adsorption of metal ions by biochar and were affected by the functional group distribution on the biochar outer and inner surfaces (see section General properties of biochar and discussion below). In the case of the analysis of Cs adsorption kinetics by the PSO model, we obtained the lowest value of the correlation coefficient ( $R^2 = 0.690$ ), the reason is mainly due to the low affinity of the monovalent ions for the negatively charged functional groups of the GW biochar.

Additionally, the multilinear relationship in the plot of  $Q_t$  vs  $t^{0.5}$  over a wide range of reaction times is clearly visible (Fig. 6), indicating bulk diffusion and diffusion in the aqueous film around the particles of biochar, succeeded with diffusion in the macro-/meso- and micropores. Two linear regimes during the adsorption of Cs<sup>+</sup>, Cu<sup>2+</sup>, Ni<sup>2+</sup>, and Pb<sup>2+</sup> were observed and in all cases, the first step showed a steeper slope than the second step. Instantaneous adsorption or external surface adsorption of metal ions appeared during the first regime, and 78% of Cu ( $k_{i1} = 0.30 \pm 0.07$ ), 54% of Ni ( $k_{i1} = 0.43 \pm 0.08$ ), 85% of Pb ( $k_{i1} = 0.84 \pm 0.48$ ), and 83% of Cs ( $k_{i1} = 0.16 \pm 0.02$ ) was rapidly uptake by the

**Fig. 6** Application IDM model for the adsorption of Cs, Cu, Ni, and Pb on GW biochar. (Initial Me concentration: 100 mg L<sup>-1</sup>; pH 6.0 (Cs<sup>+</sup>), 5.2 (Cu<sup>2+</sup>), 5.6 (Ni<sup>2+</sup>), 5.0 (Pb<sup>2+</sup>); biochar dosage 2 g L<sup>-1</sup>; particle size: 0.5–1.0 mm; 25 °C)



outer surfaces of the biochar. The second regime describes slow equilibrium attainment due to intraparticle diffusion and was represented by the slow metal ions diffusion rates and only a minor fraction of Cs<sup>+</sup>, Cu<sup>2+</sup>, Ni<sup>2+</sup>, and Pb<sup>2+</sup> ions was retained by GW biochar. Similarly, Soudani et al. [42] concluded that the migration of Cd<sup>2+</sup>, Cu<sup>2+</sup>, and Zn<sup>2+</sup> ions from solution to the outer surfaces of the oak fruit shell biochar occurs rapidly at the onset of adsorption (first regime) and the last linear parts with lower slopes suggest that the intraparticle diffusion rate of metal ions decreases and the equilibrium is reached gradually.

### Effect of pH and metal speciation

The effect of initial pH on Cs, Cu, Ni, and Pb adsorption by biochar is depicted in Fig. 7A–D together with the results of metal speciation modeling. It is evident that the adsorption of studied metal ions is a pH-dependent process since the biochar surface charge, as well as Cu, Ni, and Pb speciation, are strongly impacted by the solution pH. The pH (and H<sup>+</sup>) play a multiple role in metal adsorption. First, the solution pH affects oxygen-containing functional moieties (particularly carboxyl and hydroxyl) dissociation on the surfaces of biochar [43]. Second, pH value strongly influences solution chemistry and metal speciation. Third, the H<sup>+</sup> ion can compete with metals for biochar binding sites.

The Cu removal efficiency gradually increased from 6.7 to 27.9% with increasing initial pH of the solution from 2.0

to 5.0 followed by a sharp increase at pH 6.0, when the maximum removal efficiency (56.8%) was observed (Fig. 7A). In the case of Pb adsorption, removal efficiency significantly increased from pH 2.0 to 3.5, and then modestly increased from 4.0 to 5.0. A further steep rise in Pb adsorption was observed above pH 5.0 with maximum removal efficiency at pH 6.5 (84.8%) (Fig. 7B). Ni removal efficiency sharply increased to 9.2% at pH 3.5, stayed stabilized up to pH 7.5 and then again slightly raised. Maximum efficiency (21.5%) was reached at pH 8.5 (Fig. 7C). Cesium adsorption efficiency progressively enhanced with increasing pH at the range of 2.0–4.0 and then remained unaffected up to pH 8.0 (Fig. 7D). Lower adsorption at pH 2.0–3.0 is clearly associated with the protonation of biochar functional moieties, leading to intense competition for adsorption sites between Cs<sup>+</sup>, Cu<sup>2+</sup>, Ni<sup>2+</sup>, Pb<sup>2+</sup> and H<sup>+</sup> ions. As the pH of the solution increases, a gradual deprotonation occurs (acid alcohols and carboxylic acids lose protons) and the surface of the biochar becomes more negatively charged, resulting in a gradual increase in metal removal efficiency [44]. The reduced removal efficacy at lower pH values may be also ascribed to the electrostatic repulsion between the positively charged GW biochar (pH<sub>pzc</sub> = 7.2) and Cs<sup>+</sup>, Cu<sup>2+</sup>, Ni<sup>2+</sup>, and Pb<sup>2+</sup> ions.

The copper speciation as a function of pH in single adsorption system (Fig. 7A) indicates that hydroxide complexes become important with increasing pH values (Cu<sub>2</sub>(OH)<sub>2</sub><sup>2+</sup>; Cu(OH)<sub>3</sub><sup>-</sup>; Cu<sub>2</sub>(OH)<sub>4</sub><sup>2+</sup>; Cu(OH)<sub>2</sub>(aq)) and



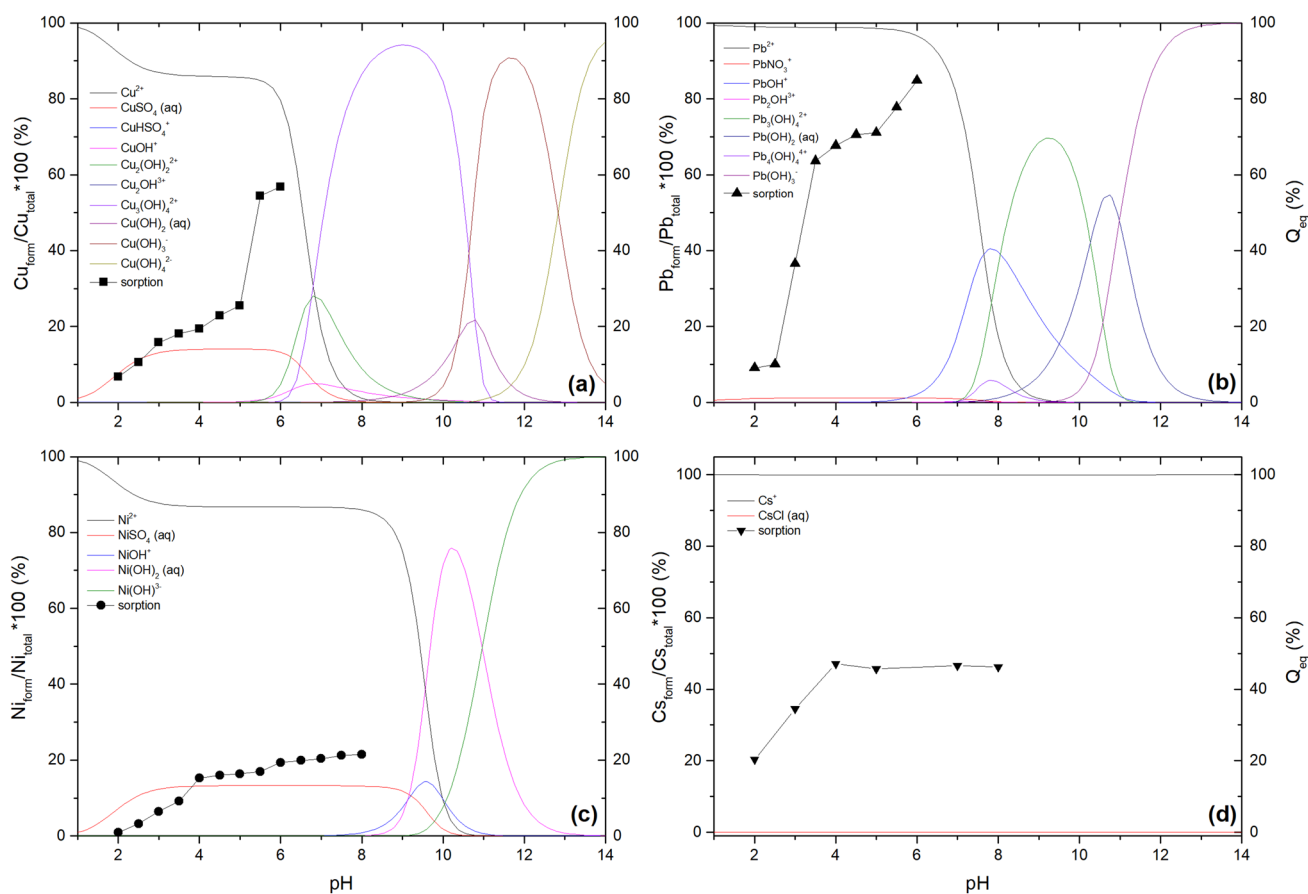


**Fig. 7** Effect of initial pH on equilibrium sorption of Cu, Pb and Ni ( $100 \text{ mg L}^{-1}$ ) and Cs ( $66 \text{ mg L}^{-1}$ ) by GW biochar and predicted Cu, Pb, Ni, and Cs speciation in aqueous solution as a function of pH at  $25^\circ \text{C}$

the precipitation of copper starts at  $\text{pH} > 6.0$ . The  $\text{Cu}^{2+}$  ions exist mostly at  $\text{pH} 2.0$  to  $5.5$  (92 to 84%). The speciation of lead is shown in Fig. 7B. Under low-pH conditions (2.0–6.0) lead is dominantly present as a divalent cation. Hydroxide complexes ( $\text{Pb}(\text{OH})_3^-$ ;  $\text{Pb}(\text{OH})^+$ ;  $\text{Pb}_3(\text{OH})_4^{2+}$ ) become important with increasing pH values and precipitation as a result of  $\text{Pb}(\text{OH})_2$  formation starting at  $\text{pH} > 7.0$ . Figure 7C illustrates Ni speciation as a function of pH for a single adsorption system. Nickel is predominantly available as  $\text{Ni}^{2+}$  ions (93–87%) under low-pH conditions (2.0–7.5). The formation of insoluble hydroxides ( $\text{Ni}(\text{OH})_2$  (aq)) starts at  $\text{pH} > 8.0$ . Further ionic species such as  $\text{Ni}(\text{OH})^+$ , and  $\text{Ni}(\text{OH})_3^-$  are available in solution at  $\text{pH} 8.0$ – $12.0$ . It is evident that the presence of cationic hydroxides of Cu and Pb and the formation of precipitates affected the adsorption process (Fig. 7A, B). Cesium exists in solution predominantly as  $\text{Cs}^+$  ion (99%) (Fig. 7D) indicating that Cs speciation has no significant effect on Cs adsorption.

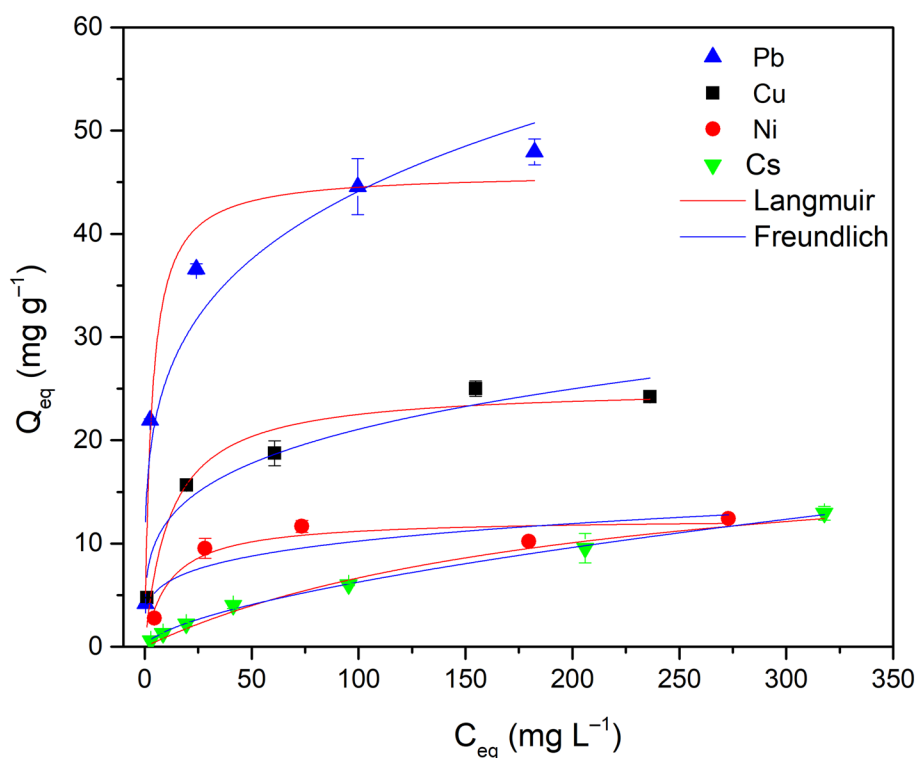
Considering the occurrence of alkali constituents in GW biochar pyrolyzed at  $500^\circ \text{C}$  the solution equilibrium pH rose after the adsorption, for instance from the initial values 3.0, 4.0, 5.5, and 6.5 to 5.5, 6.5, 6.7, and 7.2 (Ni), 4.6,

5.5, 6.1, and 7.1 (Pb), and 4.3, 5.0, 5.3, and 6.7 (Cu). In cesium sorption, the initial pH shifted from 2.0, 3.0, 4.0, and 5.0 to 3.2, 5.2, 6.5, and 7.3. Significantly higher Cu and Pb removal efficacy observed at  $\text{pH}_{\text{in}} 6.0$  and  $6.5$  respectively is presumably also due to high inner pH in the pore structure of biochar which results in both Pb and Cu microprecipitation directly on biochar outer and inner surfaces. Nzediegwu et al. [45] revealed that biochars and hydrochars with low pH values ( $< 5.0$ ) are the least effective in the removal of Pb and conversely, as the pH of biochars increases ( $> 8.0$ ), their ability to adsorb lead increases significantly. According to Wei et al. [46] the increase in biochar pH is conducive to Cu precipitation. Using the XRD analysis revealed the formation of langite ( $\text{Cu}_4(\text{SO}_4)(\text{OH})_6 \cdot 2\text{H}_2\text{O}$ ) at the surface of biochar from artichoke stalks produced at  $500^\circ \text{C}$ .

### Adsorption equilibrium of Cs, Cu, Ni, and Pb

Equilibrium adsorption trials were conducted in batch mode ( $C_{0\text{Me}} 10$ – $300 \text{ mg L}^{-1}$ ;  $C_{0\text{Cs}} 13$ – $400 \text{ mg L}^{-1}$ ; initial pH 6.0; equilibrium time 24 h; particle size 0.5–1.0 mm;  $25^\circ \text{C}$ ) to determine the removal capacities of Cs, Cu, Ni, and Pb

**Fig. 8** Langmuir and Freundlich isotherm for Cs, Cu, Ni, and Pb adsorption by GW biochar (Initial Cu, Ni, Pb concentration 10–300 mg L<sup>-1</sup>, initial Cs concentration 13–400 mg L<sup>-1</sup>, pH 6.0, biochar dosage 2 g L<sup>-1</sup>, particle size: 0.5–1.0 mm, 25 °C)



using the garden waste biochar. Isotherm models according to Langmuir's (Eq. 4) and Freundlich's (Eq. 5) were adopted to obtain quantitative information on the adsorption of studied metals. Figure 8 depicts the nonlinear fitting results, and Table 3 lists the isotherm parameters acquired. Adsorption of Ni and Pb by GW biochar provides a saturation shape of the curve (Langmuir-type isotherm), whereas the Freundlich model was well fitted to Cs and Cu adsorption data (slopes decrease when both Cs and Cu concentrations increase). The Freundlich constant  $1/n$  was  $< 1$ , stating that the adsorption isotherm belongs to the L type. The  $1/n$  value is between 0.1 and 0.7, suggesting that the adsorption of both Cs and Cu on the surface of GW biochar was facile. Higher  $R^2$  values for the Langmuir model imply that the adsorption of both Ni and Pb is attributable to the Langmuir mechanism of surface adsorption. The calculated maximum adsorption biochar capacity  $Q_{max}$ , for Ni, gained from the Langmuir model was  $12.4 \pm 0.93$  mg g<sup>-1</sup>, for Pb  $45.9 \pm 2.1$  mg g<sup>-1</sup>, for

Cu  $25.2 \pm 2.1$  mg g<sup>-1</sup>, and for Cs  $20.2 \pm 2.8$  mg g<sup>-1</sup>. The affinity parameter  $b$  refers to the initial gradient implying the affinity of GW biochar at lower concentrations of Cu, Cs, Ni, and Pb [43]. A higher affinity parameter responds to the stronger initial gradient. Clearly, lead isotherm is sharper at low Pb equilibrium concentrations compared to the isotherms attained for Cs, Cu, and Ni (Fig. 8). Reflecting  $b$  values, GW biochar exhibited a considerably elevated affinity for Pb ( $0.31$  L mg<sup>-1</sup>) in comparison with Ni ( $0.089$  L mg<sup>-1</sup>), Cu ( $0.085$  L mg<sup>-1</sup>), and Cs ( $0.001$  L mg<sup>-1</sup>).

It is apparent from Table 4 that the Langmuir adsorption capacities of GW biochar for Cs, Cu, and Pb are comparable to other biochars produced from different feedstocks. The observed adsorption capacity for Ni is noticeably lower compared to other biochar. However, it must be stressed here that it is difficult to equate the effectiveness of biochar-based adsorbents since, as can be seen from Table 4, the biochar preparation and experimental conditions vary considerably.

**Table 3** Adsorption isotherm parameters ( $\pm$ SD) for Cs, Cu, Ni, and Pb adsorption by GW biochar

Metal	Langmuir			Freundlich		
	$Q_{max}$ [mg g <sup>-1</sup> ]	$b$ [L mg <sup>-1</sup> ]	$R^2$	$K$ [mg g <sup>-1</sup> (L mg <sup>-1</sup> ) <sup>1/n</sup> ]	$1/n$	$R^2$
Cu	$25.2 \pm 2.1$	$0.085 \pm 0.041$	0.940	$6.80 \pm 1.40$	$0.25 \pm 0.04$	0.955
Ni	$12.4 \pm 0.93$	$0.089 \pm 0.037$	0.928	$3.70 \pm 1.72$	$0.22 \pm 0.10$	0.736
Pb	$45.9 \pm 2.1$	$0.31 \pm 0.08$	0.979	$15.1 \pm 3.75$	$0.23 \pm 0.06$	0.919
Cs	$20.5 \pm 2.8$	$0.005 \pm 0.001$	0.986	$0.37 \pm 0.04$	$0.62 \pm 0.02$	0.998

**Table 4** Comparison of Langmuir maximum adsorption capacities ( $Q_{max}$ ) of GW biochar for Cs, Cu, Ni, and Pb versus other biochars from different feedstocks

Metal	Biochar feedstock	Temperature (°C)/ Residence time (h)	Concentration range (mg L <sup>-1</sup> )	Contact time (h)	Adsorption capac- ity (mg g <sup>-1</sup> )	Ref.
Pb <sup>2+</sup>	Fallen leaves	450/1	0–1000	2	37.40	[47]
Pb <sup>2+</sup>	Fallen leaves + Fe solution	450/1	0–1000	2	44.62	[47]
Pb <sup>2+</sup>	Fallen leaves of <i>Platanus sp.</i>	500/4	2.3–300	24	83.30	[16]
Pb <sup>2+</sup>	Tire rubber ash	500/2	100–400	1,5	22.40	[48]
Pb <sup>2+</sup>	Corn straw	500/2	5–50	1	28.99	[49]
Pb <sup>2+</sup>	Canola straw	500/2	50–200	24	58.00	[50]
Pb <sup>2+</sup>	Garden waste	500/2	10–300	24	45.9	This study
Cu <sup>2+</sup>	Corn straw	600/2	20–250	24	12.52	[51]
Cu <sup>2+</sup>	Hardwood	450/< 1	20–250	24	6.79	[48]
Cu <sup>2+</sup>	Tire rubber ash	500/2	50–200	2	34.40	[48]
Cu <sup>2+</sup>	Almond shell	650/n. s	50–200	0.5–4	20.00	[12]
Cu <sup>2+</sup>	<i>Algae sp.</i>	600/0.5	5–400	12	14.83	[11]
Cu <sup>2+</sup>	Cedarwood	700/1	20–5000	24	28.65	[14]
Cu <sup>2+</sup>	Farmyard manure	450/1	20–5000	24	35.84	[14]
Cu <sup>2+</sup>	Rice straw	600/n. s	30–150	24	19.57	[52]
Cu <sup>2+</sup>	Pulp mill sludge	600/n. s	30–150	24	39.37	[52]
Cu <sup>2+</sup>	Garden waste	500/2	10–300	24	25.2	This study
Ni <sup>2+</sup>	Lotus stalks	400/1	20–80	48	29.90	[53]
Ni <sup>2+</sup>	Pulp mill sludge	600/n. s	30–150	24	58.48	[52]
Ni <sup>2+</sup>	Rice straw	600/n. s	30–150	24	54.95	[52]
Ni <sup>2+</sup>	Garden waste	500/2	10–300	24	12.4	This study
Cs <sup>+</sup>	Mesquite wood	900/3	20–2000	24	32.2	[9]
Cs <sup>+</sup>	Mesquite wood + food waste	900/3	20–2000	24	41.0	[9]
Cs <sup>+</sup>	Corn cobs	460/2	13–800	24	2.75	[8]
Cs <sup>+</sup>	Walnut shell	500/2	13–800	24	6.26	[8]
Cs <sup>+</sup>	Japanese oak	600–800/n.s	1–33	24	2.26	[54]
Cs <sup>+</sup>	Garden waste	500/2	13–400	24	20.5	This study

High adsorption capacities are sometimes only achieved by using very high initial metal concentrations (e.g. 2 or 5 g L<sup>-1</sup>; Table 4), which are rarely found in contaminated environments. The efficiency of these sorbents is typically substantially reduced at lower metal concentrations.

### Impact of biochar characteristics on Cs, Cu, Ni, and Pb removal

Recently, several mechanisms have been postulated for the removal of heavy metals by biochar-based adsorbents (see e.g., review by Ambaye et al. [44]). Our data indicates that the removal of Cs, Cu, Ni, and Pb by GW biochar is controlled by multiple mechanisms whereby the characteristics (physical and structural properties) of prepared biochar play an essential role.

### Oxygen-containing functional moieties

The types and content of oxygen functional moieties on biochar surfaces obtained by analysis of the O 1 s and C 1 s XPS high-resolution spectra (Fig. 2b and c) points to their important role in metal bonding. The association of Cs<sup>+</sup> ions with the carboxyl functional moiety (–C–O–Cs) deprotonated under the given experimental conditions, is mainly assumed. There is also the potential for additional stabilizing coordination to the electron pair donors or association in a cavity that contains several neutral oxygen functional moieties existing on the surface of biochar. For divalent cations, we anticipated simultaneous association of the two carboxylate anions with Me<sup>2+</sup> ions or further stabilizing interactions with the electron pairs of oxygen functional moieties [4]. This was supported by FTIR analysis (Fig. 3). After Cu<sup>2+</sup>, Ni<sup>2+</sup>, and Pb<sup>2+</sup> adsorption the peaks of carbonylic and carboxylic moieties at 1693 cm<sup>-1</sup> weakened and shifted to higher wavenumbers (1698 cm<sup>-1</sup>) confirming the

involvement of carboxylate anion in the bonding of metal cations. Similarly, Wang et al. [55] describe the role of O-containing moieties of walnut shell biochar in coordination with  $\text{Pb}^{2+}$  due to the surface complexation with  $-\text{COOH}$  and  $-\text{OH}$  groups. After  $\text{Cs}^+$  adsorption, the peaks of carbonylic and carboxylic groups ( $1684\text{ cm}^{-1}$ ) shift to higher wavenumbers ( $1694\text{ cm}^{-1}$ ).

### Aromatic biochar carbon

The presence of polycondensed aromatic structures in biochars produced at higher pyrolysis temperatures (our GW biochar at  $500\text{ }^\circ\text{C}$ ) enables the existence of electron-donor acceptor (EDA) interactions and the ability of aromatic ring to engage in adsorption processes. The slight shifts from  $875\text{ cm}^{-1}$  to  $869\text{ cm}^{-1}$  (Fig. 3) and changes in peak intensities (out-of-plane bending vibrations of aromatic C–H bond) may be ascribed to the interactions between  $\text{Cu}^{2+}$ ,  $\text{Ni}^{2+}$ , and  $\text{Pb}^{2+}$  ions as  $\pi$ -acceptors and polycondensed aromatic structures of GW biochar as  $\pi$ -donor [56]. Moreover, the aromatic  $\nu(\text{C}=\text{C})$  bands at  $1573\text{ cm}^{-1}$  changed after both  $\text{Cs}^+$  and  $\text{Me}^{2+}$  sorption confirming the role of  $\text{Me}^+-\pi$  EDA interactions in  $\text{Cs}^+$  adsorption and  $\text{Me}^{2+}-\pi$  EDA interactions in  $\text{Cu}^{2+}$ ,  $\text{Ni}^{2+}$  and  $\text{Pb}^{2+}$  ions adsorption (Fig. 3). Khandaker et al. [57] confirmed that beside O-functional moieties,  $\text{Cs}^+-\pi$  interaction among the aromatic  $\pi$ -system in the activated wood carbon samples and Cs in aqueous solution are involved in Cs uptake.

### Mineral constituents of the biochar

The slow pyrolysis at  $500\text{ }^\circ\text{C}$  results to the generation of pyrolysis product that contains a variety of inorganic elements (see EDX elemental mapping on Fig. 1b which are frequently found in the form of carbonates, oxides, and phosphates. As reported, sylvite (KCl), calcite ( $\text{CaCO}_3$ ), hydroxyapatite ( $\text{Ca}_5(\text{PO}_4)_3(\text{OH})$ ), amorphous silica, and quartz ( $\text{SiO}_2$ ) represent the most abundant minerals in biochars [58]. Those minerals might act as additional sites for studied metals on the biochars because of their strong adsorption affinity for  $\text{Cu}^{2+}$  [59],  $\text{Ni}^{2+}$  [60], and  $\text{Pb}^{2+}$  ions [61, 62]. Variations in peak intensities at  $1401\text{ cm}^{-1}$  (carbonate groups) and  $1027\text{ cm}^{-1}$  (P–O bond of phosphates) after adsorption of Cu and Cd suggested precipitation between  $\text{Cu}^{2+}$  and  $\text{Pb}^{2+}$  ions and  $\text{CO}_3^{2-}$  or  $\text{PO}_4^{3-}$  (Fig. 3), and peaks appearing at  $710\text{ cm}^{-1}$  are likely due to the formation of copper and lead precipitates. Zhang et al. [63] confirmed that Cd precipitated as  $\text{CdCO}_3$ ,  $\text{Cd}_3(\text{PO}_4)_2$ , and  $\text{Cd}_3\text{P}_2$  on the surface of water hyacinth-derived biochar. After Cs adsorption, significant changes were observed in the region of bandwidths  $1200$  to  $1100\text{ cm}^{-1}$  ( $\nu(\text{Si}-\text{O})$  of associated clay minerals) also indicating the participation of biochar mineral fraction on Cs sequestration. Palansooriya et al. [9]

confirmed that crystalline mineral phases of biochar (calcite, quartz, aragonite, coeruleolactite,  $\text{Ca}(\text{OH})_2$ , and  $\text{CaO}$ ) facilitated Cs adsorption. It is therefore clear that inorganic particles (Fig. 1b) present on the surface or trapped in the porous structure of GW biochar contribute to metal ions adsorption. We propose the involvement of several mechanisms in the removal of Cs, Cu, Ni, and Pb related to the mineral constituents of the biochar: (i) ion exchange of biochar-associated mineral ions ( $\text{K}^+$ ,  $\text{Na}^+$ ,  $\text{Ca}^{2+}$  or  $\text{Mg}^{2+}$ ) with  $\text{Cs}^+$  and  $\text{Me}^{2+}$ ; (ii) electrostatic attraction among negatively charged minerals and metal ions; (iii) internal complexation and co-precipitation metal ions with biochar mineral oxides, and (iv) co-precipitation of  $\text{Cs}^+$ ,  $\text{Cu}^{2+}$ ,  $\text{Ni}^{2+}$ , and  $\text{Pb}^{2+}$  ions with  $\text{SO}_4^{2-}$ ,  $\text{OH}^-$ ,  $\text{CO}_3^{2-}$ ,  $\text{SiO}_4^{4-}$  or  $\text{PO}_4^{3-}$  anions released from the minerals in biochar.

From the available measurements (FTIR, XPS, and SEM–EDX), we concluded that both the mineral and carbon fractions of GW biochar contribute to the adsorption of Cu, Ni, and Pb. In addition, except outer biochar surfaces, Cs, Cu, Ni, and Pb can be adsorbed to the pores, slits, and fissures and pores which constitute the complex biochar inner microstructure (Fig. 1a, b) and physisorption (porosity of biochar) as further removal mechanism of metal ions cannot be ignored.

However, it must be stressed here that a number of synthetic and modified adsorbents with superior selectivity and excellent adsorptive capacities have been studied for the removal of Cs [6], and other toxic metals. Large-scale applications utilizing such materials, however, can be restricted by their poor availability and comparatively high price. We, therefore, suggest that the first option could be readily obtainable sorbents for Cs and toxic metals with adequate adsorptive capacity, such as biochar, which could be employed in the form of reactive filters and barriers to avoid dispersion of the contamination. The use of biochar in the in situ decontamination of metals and radionuclides might be a more viable approach than the application of the more costly activated carbon. Nevertheless, more investigation is required to optimize the application of GW in large-scale remediation and post-treatment stabilization of biochar after the clean-up operation.

## Conclusions

Garden waste was thermochemically converted into biochar material, characterized using SEM–EDX, XPS, and FT-IR analyses and used for Cs, Cu, Ni, and Pb removal from aqueous solutions. Adsorption of Ni and Pb by GW biochar provided Langmuir-type isotherm, whereas the Freundlich isotherm was well fitted to Cs and Cu adsorption data. The biochar's capacity (Langmuir  $Q_{max}$ ) to adsorb metal ions was 20.5 (Cs), 25.2 (Cu), 12.4 (Ni), and 45.9

(Pb) mg g<sup>-1</sup> and indicated well performance for a range of pH values (3.0–6.0). EDX elemental mapping and FT-IR analysis confirmed the impact of biochar characteristics on Cs, Cu, Ni, and Pb removal. The adsorption proceeds via the formation of complexes between O-containing functional moieties, Me<sup>+</sup>-π and Me<sup>2+</sup>-π EDA interactions with the biochar electron-deficient aromatic structures, and interactions between the mineral components of biochar and metals. In conclusion, the fast adsorption kinetics and adequate adsorption capacity for the tested metal ions indicate the suitability of employing biochar from garden residues as an alternate sorbent for large volumes of wastewater polluted with heavy metals and radionuclides.

**Acknowledgments** This work was supported by the Slovak Research and Development Agency under contract number SK-AT-20-0004, the Scientific Grant Agency of the Ministry of Education, Science, Research and Sport of the Slovak Republic, project number VEGA 1/0220/23, University of Trnava in Trnava, project number 4/TU/2022 and Faculty of Education, university of Trnava in Trnava, project number C1/2022.

**Funding** Open access funding provided by The Ministry of Education, Science, Research and Sport of the Slovak Republic in cooperation with Centre for Scientific and Technical Information of the Slovak Republic. Agentúra na Podporu Výskumu a Vývoja, SK-AT-20-0004, Vladimír Frišták, Agentúra Ministerstva Školstva, Vedy, Výskumu a Športu SR, 01/0220/23, Trnavská univerzita v Trnave, 4/TU/2022, Vladimír Frišták, Pedagogická fakulta, Trnavská univerzita v Trnave, C1/2022, Martin Pipiška.

## Declarations

**Conflict of interest** There were no known conflict of interest or personal relationships that could have appeared to influence the work reported in this paper.

**Open Access** This article is licensed under a Creative Commons Attribution 4.0 International License, which permits use, sharing, adaptation, distribution and reproduction in any medium or format, as long as you give appropriate credit to the original author(s) and the source, provide a link to the Creative Commons licence, and indicate if changes were made. The images or other third party material in this article are included in the article's Creative Commons licence, unless indicated otherwise in a credit line to the material. If material is not included in the article's Creative Commons licence and your intended use is not permitted by statutory regulation or exceeds the permitted use, you will need to obtain permission directly from the copyright holder. To view a copy of this licence, visit <http://creativecommons.org/licenses/by/4.0/>.

## References

- Vijay V, Shreedhar S, Adlak K, Payyanad S, Sreedharan V, Gopi G, Voort ST, Malarvizhi P, Yi S, Gebert J, Aravind P (2021) Review of large-scale biochar field-trials for soil amendment and the observed influences on crop yield variations. *Front Energy Res* 9:710766. <https://doi.org/10.3389/fenrg.2021.710766>
- Yang Y, Sun K, Liu J, Chen Y, Han L (2022) Changes in soil properties and CO<sub>2</sub> emissions after biochar addition: role of pyrolysis temperature and aging. *Sci Total Environ* 839:156333. <https://doi.org/10.1016/j.scitotenv.2022.156333>
- Majumder S, Neogi S, Dutta T, Powel MA, Banik P (2019) The impact of biochar on soil carbon sequestration: meta-analytical approach to evaluating environmental and economic advantages. *J Environ Manage* 250:109466. <https://doi.org/10.1016/j.jenvman.2019.109466>
- Ballová S, Pipiška M, Frišták V, Ďuriška L, Horník M, Kaňuchová M, Soja G (2020) Pyrogenic carbon for decontamination of low-level radioactive effluents: simultaneous separation of <sup>137</sup>Cs and <sup>60</sup>Co. *Prog Nucl Energy* 129:103484. <https://doi.org/10.1016/j.pnucene.2020.103484>
- Sayin F, Akar ST, Akar T (2021) From green biowaste to water treatment applications: utilization of modified new biochar for the efficient removal of ciprofloxacin. *Sustain Chem Pharm* 24:100522. <https://doi.org/10.1016/j.scp.2021.100522>
- Liu H, Tong L, Su M, Chen D, Song G, Zhou Y (2023) The latest research trends in the removal of cesium from radioactive wastewater: a review based on data-driven and visual analysis. *Sci Total Environ* 869:161664. <https://doi.org/10.1016/j.scitotenv.2023.161664>
- Saarela T, Lafdani EK, Laurén A, Pumpanen J, Palviainen M (2020) Biochar as adsorbent in purification of clear-cut forest runoff water: adsorption rate and adsorption capacity. *Biochar* 2(2):227–237. <https://doi.org/10.1007/s42773-020-00049-z>
- Pipiška M, Ballová S, Frišták V, Ďuriška L, Horník M, Demčák Š, Holub M, Soja G (2020) Assessment of pyrogenic carbonaceous materials for effective removal of radiocesium. *Key Eng Mater* 838:103–110. <https://doi.org/10.4028/www.scientific.net/KEM.838.103>
- Palansooriya KN, Yoon I-H, Kim S-M, Wang C-H, Kwon H, Lee S-H, Igalavithana AD, Mukhopadhyay R, Sarkar B, Ok YS (2022) Designer biochar with enhanced functionality for efficient removal of radioactive cesium and strontium from water. *Environ Res* 214:114072. <https://doi.org/10.1016/j.envres.2022.114072>
- Ahmed W, Mehmood S, Núñez-Delgado A, Qaswar M, Ali S, Ying H, Liu Z, Mahmood M, Chen D-Y (2021) Fabrication, characterization and U(VI) sorption properties of a novel biochar derived from *Tribulus terrestris* via two different approaches. *Sci Total Environ* 780:146617. <https://doi.org/10.1016/j.scitotenv.2021.146617>
- Jin H, Hanif MU, Capareda S, Chang Z, Huang H, Ai Y (2016) Copper(II) removal potential from aqueous solution by pyrolysis biochar derived from anaerobically digested algae-dairy-manure and effect of KOH activation. *J Environ Chem Eng* 4(1):365–372. <https://doi.org/10.1016/j.jece.2015.11.022>
- Kılıç M, Kırbıyık Ç, Çepeliogullar Ö, Pütün AE (2013) Adsorption of heavy metal ions from aqueous solutions by bio-char, a by-product of pyrolysis. *Appl Surf Sci* 283:856–862. <https://doi.org/10.1016/j.apsusc.2013.07.033>
- Park SH, Cho HJ, Ryu C, Park Y-K (2016) Removal of copper(II) in aqueous solution using pyrolytic biochars derived from red macroalga *Porphyra tenera*. *J Ind Eng Chem* 36:314–319. <https://doi.org/10.1016/j.jiec.2016.02.021>
- Rodríguez-Vila A, Selwyn-Smith H, Enunwa L, Smail I, Covelo EF, Sizmur T (2018) Predicting Cu and Zn sorption capacity of biochar from feedstock C/N ratio and pyrolysis temperature. *Environ Sci Pollut Res* 25(8):7730–7739. <https://doi.org/10.1007/s11356-017-1047-2>
- Alhashimi HA, Aktas CB (2017) Life cycle environmental and economic performance of biochar compared with activated carbon: a meta-analysis. *Resour Conserv Recycl* 118:13–26. <https://doi.org/10.1016/j.resconrec.2016.11.016>
- Park J-H, Wang JJ, Xiao R, Wang M, Lee YH, Kang SW, Seo D-C (2022) Characteristics of adsorption behavior of potentially toxic metals by biochar derived from fallen leaves (*Platanus*) and

- its mechanism. *Sustain Chem Pharm* 29:100776. <https://doi.org/10.1016/j.scp.2022.100776>
17. Zhou R, Zhang M, Shao S (2022) Optimization of target biochar for the adsorption of target heavy metal ion. *Sci Rep* 12(1):1. <https://doi.org/10.1038/s41598-022-17901-w>
  18. Awad M, Moustafa-Farag M, Wei L, Huang Q, Liu Z (2020) Effect of garden waste biochar on the bioavailability of heavy metals and growth of *Brassica juncea* (L.) in a multi-contaminated soil. *Arab J Geosci* 13(12):439. <https://doi.org/10.1007/s12517-020-05376-w>
  19. Cui S, Ke Y, Fu Q, Hough R, Zhang Z, Shen Z, An L, Li Y-F (2022) Optimization preparation of biochar from garden waste and quantitative analysis for Cd<sup>2+</sup> adsorption mechanism in aqueous solution. *Biomass Convers Biorefin*. <https://doi.org/10.1007/s13399-022-03289-0>
  20. Houssou AA, Jeyakumar P, Niazi NK, Van Zwieten L, Li X, Huang L, Wei L, Zheng X, Huang Q, Huang Y, Huang X, Wang H, Liu Z, Huang Z (2022) Biochar and soil properties limit the phytoavailability of lead and cadmium by *Brassica chinensis* L. in contaminated soils. *Biochar* 4(1):5. <https://doi.org/10.1007/s42773-021-00126-x>
  21. Pipířka M, Krajčířková EK, Hvostik M, Friřták V, Ďuriřka L, Āerničková I, Kaňuchová M, Conte P, Soja G (2022) Biochar from wood chips and corn cobs for adsorption of thioflavin T and erythrosine B. *Materials* 15(4):1492. <https://doi.org/10.3390/ma15041492>
  22. Ho YS, McKay G (1999) Pseudo-second order model for sorption processes. *Process Biochem* 34(5):451–465. [https://doi.org/10.1016/S0032-9592\(98\)00112-5](https://doi.org/10.1016/S0032-9592(98)00112-5)
  23. Weber WJ, Morris JC (1963) Kinetics of adsorption on carbon from solution. *J Sanit Eng Div* 89:31–59
  24. Langmuir I (1918) The adsorption of gases on plane surfaces of glass, mica and platinum. *J Am Chem Soc* 40(9):1361–1403. <https://doi.org/10.1021/ja02242a004>
  25. Freundlich H (1907) Über die adsorption in Lösungen. *Z fur Phys Chem* 57U(1):385–470. <https://doi.org/10.1515/zpch-1907-5723>
  26. Visual MINTEQ – Visual MINTEQ – a free equilibrium speciation model. Cit 03. november 2022. <https://vminteq.lwr.kth.se/>
  27. Pradhan S, Abdelaal AH, Mroue K, Al-Ansari T, Mackey HR, McKay G (2020) Biochar from vegetable wastes: agro-environmental characterization. *Biochar* 2(4):439–453. <https://doi.org/10.1007/s42773-020-00069-9>
  28. Liu W-J, Jiang H, Yu H-Q (2015) Development of biochar-based functional materials: toward a sustainable platform carbon material. *Chem Rev* 115(22):12251–12285. <https://doi.org/10.1021/acs.chemrev.5b00195>
  29. Vijayaraghavan K (2021) The importance of mineral ingredients in biochar production, properties and applications. *Crit Rev Environ Sci Technol* 51(2):113–139. <https://doi.org/10.1080/10643389.2020.1716654>
  30. Clemente JS, Beauchemin S, Thibault Y, MacKinnon T, Smith D (2018) Differentiating inorganics in biochars produced at commercial scale using principal component analysis. *ACS Omega* 3(6):6931–6944. <https://doi.org/10.1021/acsomega.8b00523>
  31. Pipířka M, Ballová S, Friřták V, Ďuriřka L, Horník M, Demcak S, Holub M, Soja G (2020) Potassium nickel(II) hexacyanoferrate(III)-functionalized biochar for selective separation of radiocesium from liquid wastes. *J Radiat Res Appl Sci* 13:343–355. <https://doi.org/10.1080/16878507.2020.1740394>
  32. Zhang L, Jing Y, Chen G, Wang X, Zhang R (2019) Improvement of physical and hydraulic properties of desert soil with amendment of different biochars. *J Soil Sedim* 19(7):2984–2996. <https://doi.org/10.1007/s11368-019-02293-8>
  33. Aarva A, Deringer VL, Sainio S, Laurila T, Caro MA (2019) Understanding X-ray spectroscopy of carbonaceous materials by combining experiments, density functional theory, and machine learning. Part II: quantitative fitting of spectra. *Chem Mater* 31:9256–9267. <https://doi.org/10.1021/acs.chemmater.9b02050>
  34. Zielke U, Hüttinger KJ, Hoffman WP (1996) Surface-oxidized carbon fibers: I. *Surf Struct Chem Carbon* 34(8):983–998. [https://doi.org/10.1016/0008-6223\(96\)00032-2](https://doi.org/10.1016/0008-6223(96)00032-2)
  35. Kloss S, Zehetner F, Dellantonio A, Hamid R, Ottner F, Liedtke V, Schwanninger M, Gerzabek MH, Soja G (2012) Characterization of slow pyrolysis biochars: effects of feedstocks and pyrolysis temperature on biochar properties. *J Environ Qual* 41(4):990–1000. <https://doi.org/10.2134/jeq2011.0070>
  36. Berek AK, Hue NV (2016) Characterization of biochars and their use as an amendment to acid soils. *Soil Sci* 181(9/10):412–426. <https://doi.org/10.1097/SS.0000000000000177>
  37. Zhao S-X, Ta N, Wang X-D (2017) Effect of temperature on the structural and physicochemical properties of biochar with apple tree branches as feedstock material. *Energies* 10(9):1293. <https://doi.org/10.3390/en10091293>
  38. Liu J, Wang H, Ma N, Zhou B, Chen H, Yuan R (2022) Optimization of the raw materials of biochars for the adsorption of heavy metal ions from aqueous solution. *Water Sci Technol* 85(10):2869–2881. <https://doi.org/10.2166/wst.2022.158>
  39. Mahdi Z, Yu QJ, El Hanandeh A (2018) Investigation of the kinetics and mechanisms of nickel and copper ions adsorption from aqueous solutions by date seed derived biochar. *J Environ Chem Eng* 6(1):1171–1181. <https://doi.org/10.1016/j.jece.2018.01.021>
  40. Sakhiya AK, Vijay VK, Kaushal P (2022) Efficacy of rice straw derived biochar for removal of Pb<sup>2+</sup> and Zn<sup>2+</sup> from aqueous: adsorption, thermodynamic and cost analysis. *Bioresour Technol Rep* 17:100920. <https://doi.org/10.1016/j.biteb.2021.100920>
  41. Xiang A, Gao Z, Zhang K, Jiang E, Ren Y, Wang M (2021) Study on the Cd (II) adsorption of biochar based carbon fertilizer. *Ind Crop Prod* 174:114213. <https://doi.org/10.1016/j.indcrop.2021.114213>
  42. Soudani A, Youcef L, Bulgariu L, Youcef S, Toumi K, Soudani N (2022) Characterizing and modeling of oak fruit shells biochar as an adsorbent for the removal of Cu, Cd, and Zn in single and in competitive systems. *Chem Eng Res Des* 188:972–987. <https://doi.org/10.1016/j.cherd.2022.10.009>
  43. Pipířka M, Richevisová BM, Friřták V, Horník M, Remenářová L, Stiller R, Soja G (2017) Sorption separation of cobalt and cadmium by straw-derived biochar: a radiometric study. *J Radioanal Nucl Chem* 311(1):85–97. <https://doi.org/10.1007/s10967-016-5043-7>
  44. Ambaye TG, Vaccari M, van Hullebusch ED, Amrane A, Rtimi S (2021) Mechanisms and adsorption capacities of biochar for the removal of organic and inorganic pollutants from industrial wastewater. *Int J Environ Sci Technol* 18(10):3273–3294. <https://doi.org/10.1007/s13762-020-03060-w>
  45. Nzediegwu C, Naeth MA, Chang SX (2021) Lead(II) adsorption on microwave-pyrolyzed biochars and hydrochars depends on feedstock type and production temperature. *J Haz Mater* 412:125255. <https://doi.org/10.1016/j.jhazmat.2021.125255>
  46. Wei J, Tu C, Yuan G, Liu Y, Bi D, Xiao L, Lu J, Theng BKG, Wang H, Zhang L, Zhang X (2019) Assessing the effect of pyrolysis temperature on the molecular properties and copper sorption capacity of a halophyte biochar. *Environ Pollut* 251:56–65. <https://doi.org/10.1016/j.envpol.2019.04.128>
  47. Wang C, Wang H (2018) Pb(II) sorption from aqueous solution by novel biochar loaded with nano-particles. *Chemosphere* 192:1–4. <https://doi.org/10.1016/j.chemosphere.2017.10.125>
  48. Mousavi HZ, Hosseynifar A, Jahed V, Dehghani SAM (2010) Removal of lead from aqueous solution using waste tire rubber ash as an adsorbent. *Braz J Chem Eng* 27(1):79–87. <https://doi.org/10.1590/S0104-66322010000100007>
  49. Chi T, Zuo J, Liu F (2017) Performance and mechanism for cadmium and lead adsorption from water and soil by corn straw

- biochar. *Front Environ Sci Eng* 11(2):15. <https://doi.org/10.1007/s11783-017-0921-y>
50. Kwak J-H, Islam MS, Wang S, Messele SA, Naeth MA, El-Din MG, Chang SX (2019) Biochar properties and lead(II) adsorption capacity depend on feedstock type, pyrolysis temperature, and steam activation. *Chemosphere* 231:393–404. <https://doi.org/10.1016/j.chemosphere.2019.05.128>
51. Chen L-F, Liang H-W, Lu Y, Cui C-H, Yu S-H (2011) Synthesis of an attapulgite clay@carbon nanocomposite adsorbent by a hydrothermal carbonization process and their application in the removal of toxic metal ions from water. *Langmuir* 27(14):8998–9004. <https://doi.org/10.1021/la2017165>
52. Islam MS, Kwak J-H, Nzediegwu C, Wang S, Palansuriya K, Kwon EE, Naeth MA, El-Din MG, Ok YS, Chang SX (2021) Biochar heavy metal removal in aqueous solution depends on feedstock type and pyrolysis purging gas. *Environ Pollut* 281:117094. <https://doi.org/10.1016/j.envpol.2021.117094>
53. Liu H, Liang S, Gao J, Ngo HH, Guo W, Guo Z, Li Y (2014) Development of biochars from pyrolysis of lotus stalks for Ni(II) sorption: using zinc borate as flame retardant. *J Anal Appl Pyrol* 107:336–341. <https://doi.org/10.1016/j.jaap.2014.02.018>
54. Yamauchi S, Yamagishi T, Kirikoshi K, Yatagai M (2014) Cesium adsorption from aqueous solutions onto Japanese oak charcoal I: effects of the presence of group 1 and 2 metal ions. *J Wood Sci* 60(6):473–479. <https://doi.org/10.1007/s10086-014-1431-1>
55. Wang Z, Liu G, Zheng H, Li F, Ngo HH, Guo W, Liu C, Chen L, Xing B (2015) Investigating the mechanisms of biochar's removal of lead from solution. *Bioresour Technol* 177:308–317. <https://doi.org/10.1016/j.biortech.2014.11.077>
56. Liu T, Chen Z, Li Z, Chen G, Zhou J, Chen Y, Zhu J, Chen Z (2021) Rapid separation and efficient removal of Cd based on enhancing surface precipitation by carbonate-modified biochar. *ACS Omega* 6(28):18253–18259. <https://doi.org/10.1021/acsomega.1c02126>
57. Khandaker S, Chowdhury MF, Awual MR, Islam A, Kuba T (2021) Efficient cesium encapsulation from contaminated water by cellulosic biomass based activated wood charcoal. *Chemosphere* 262:127801. <https://doi.org/10.1016/j.chemosphere.2020.127801>
58. Xu Y, Liang X, Xu Y, Qin X, Huang Q, Wang L, Sun Y (2017) Remediation of heavy metal-polluted agricultural soils using clay minerals: a review. *Pedosphere* 27(2):193–204. [https://doi.org/10.1016/S1002-0160\(17\)60310-2](https://doi.org/10.1016/S1002-0160(17)60310-2)
59. Kong L, Liu X, Lv G, Liu T, Zhang P, Li Y, Chen B, Liao L (2022) Copper adsorption using hydroxyapatite derived from bovine bone. *Adv Civil Eng*. <https://doi.org/10.1155/2022/1026129>
60. Belova DA, Lakshtanov LZ, Carneiro JF, Stipp SLS (2014) Nickel adsorption on chalk and calcite. *J Contam Hydrol* 170:1–9. <https://doi.org/10.1016/j.jconhyd.2014.09.007>
61. Fiorito E, Porcedda GE, Brundu L, Passiu C, Atzei D, Ennas G, Elsener B, Fantauzzi M, Rossi A (2022) Calcium carbonate as sorbent for lead removal from wastewaters. *Chemosphere* 296:133897. <https://doi.org/10.1016/j.chemosphere.2022.133897>
62. Wang H, Lv Z, Wang Y, Sun Y, Tsang YF (2021) Recycling of biogenic hydroxyapatite (HAP) for cleaning of lead from wastewater: performance and mechanism. *Environ Sci Pollut Res* 28(23):29509–29520. <https://doi.org/10.1007/s11356-020-10855-4>
63. Zhang F, Wang X, Yin D, Peng B, Tan C, Liu Y, Tan X, Wu S (2015) Efficiency and mechanisms of Cd removal from aqueous solution by biochar derived from water hyacinth (*Eichornia crassipes*). *J Environ Manage* 153:68–73. <https://doi.org/10.1016/j.jenvman.2015.01.043>

**Publisher's Note** Springer Nature remains neutral with regard to jurisdictional claims in published maps and institutional affiliations.